Article

Cell Reports

Autism-like Deficits in *Shank3*-Deficient Mice Are Rescued by Targeting Actin Regulators

Graphical Abstract

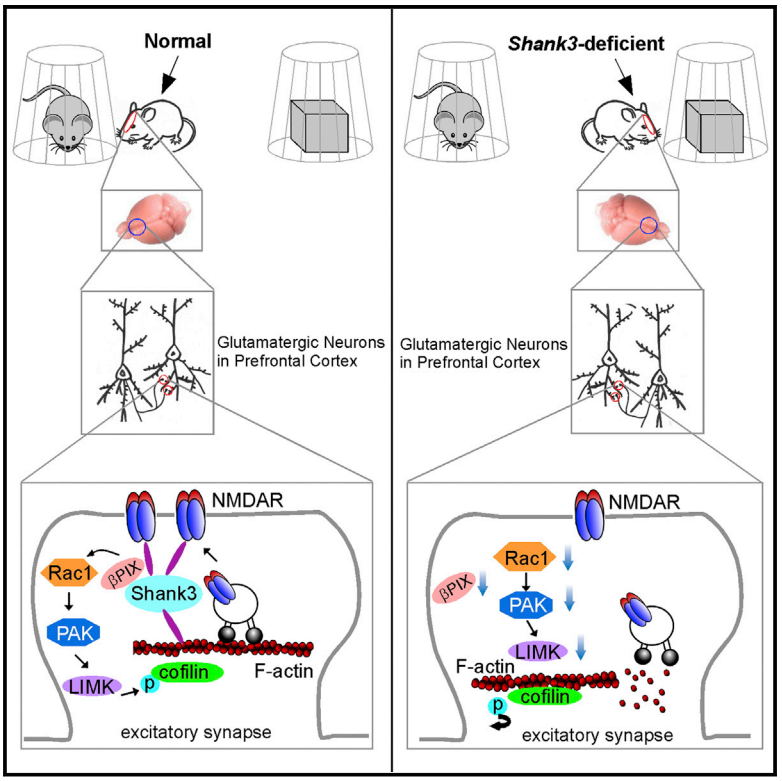

Highlights

- *Shank3* deficiency induces ASD-like behavioral deficits and NMDAR hypofunction in PFC
- *Shank3* deficiency leads to reduced synaptic F-actin and altered actin regulators in PFC
- Inhibiting cofilin rescues behavioral and synaptic deficits in *Shank3*-deficient mice
- Manipulating cortical Rac1 or PAK controls the manifestation of ASD-like phenotypes

Authors

Lara J. Duffney, Ping Zhong, ..., Joseph D. Buxbaum, Zhen Yan

Correspondence

zhenyan@buffalo.edu

In Brief

Shank3 haploinsufficiency is an autism risk factor. Duffney et al. reveal that *Shank3* deficiency causes the diminished synaptic actin filaments and NMDA receptors in prefrontal cortex. Targeting key actin regulators, including cofilin, Rac1, and PAK, rescues the autism-like behavioral and synaptic deficits, which provides a strategy for autism treatment.

Duffney et al., 2015, Cell Reports *11*, 1400–1413
June 9, 2015 ©2015 The Authors
http://dx.doi.org/10.1016/j.celrep.2015.04.064

OPEN ACCESS
CellPress

Cell Reports
Article

Autism-like Deficits in *Shank3*-Deficient Mice Are Rescued by Targeting Actin Regulators

Lara J. Duffney,[1,4] Ping Zhong,[1,4] Jing Wei,[1,4] Emmanuel Matas,[1] Jia Cheng,[1] Luye Qin,[1] Kaijie Ma,[1] David M. Dietz,[2] Yuji Kajiwara,[3] Joseph D. Buxbaum,[3] and Zhen Yan[1,*]

[1]Department of Physiology and Biophysics, State University of New York at Buffalo, Buffalo, NY, 14214, USA
[2]Department of Pharmacology and Toxicology, State University of New York at Buffalo, Buffalo, NY, 14214, USA
[3]Seaver Autism Center for Research and Treatment, Department of Psychiatry, Friedman Institute and Mindich Child Health and Development Institute, Icahn School of Medicine at Mount Sinai, New York, NY 10029, USA
[4]Co-first author
*Correspondence: zhenyan@buffalo.edu
http://dx.doi.org/10.1016/j.celrep.2015.04.064
This is an open access article under the CC BY-NC-ND license (http://creativecommons.org/licenses/by-nc-nd/4.0/).

SUMMARY

Haploinsufficiency of the *Shank3* gene, which encodes a scaffolding protein at glutamatergic synapses, is a highly prevalent and penetrant risk factor for autism. Using combined behavioral, electrophysiological, biochemical, imaging, and molecular approaches, we find that *Shank3*-deficient mice exhibit autism-like social deficits and repetitive behaviors, as well as the significantly diminished NMDA receptor (NMDAR) synaptic function and synaptic distribution in prefrontal cortex. Concomitantly, *Shank3*-deficient mice have a marked loss of cortical actin filaments, which is associated with the reduced Rac1/PAK activity and increased activity of cofilin, the major actin depolymerizing factor. The social deficits and NMDAR hypofunction are rescued by inhibiting cofilin or activating Rac1 in *Shank3*-deficient mice and are induced by inhibiting PAK or Rac1 in wild-type mice. These results indicate that the aberrant regulation of synaptic actin filaments and loss of synaptic NMDARs contribute to the manifestation of autism-like phenotypes. Thus, targeting actin regulators provides a strategy for autism treatment.

INTRODUCTION

Autism spectrum disorder (ASD) is a group of neurodevelopmental disorder characterized by impaired social communication and repetitive and restricted behavioral patterns. Haploinsufficiency of the *Shank3* gene due to deletion or de novo mutation has been linked to autism in human genetics studies (Bonaglia et al., 2001; Durand et al., 2007; Sebat et al., 2007; Betancur and Buxbaum, 2013; De Rubeis et al., 2014) and animal model investigations (Bozdagi et al., 2010; Wang et al., 2011; Peça et al., 2011; Kouser et al., 2013). Shank3 is a scaffolding protein at postsynaptic density (PSD) of glutamatergic synapses and includes an N-terminal ankyrin repeat domain, a SH3 domain, a PDZ domain that links to guanylate kinase-associated proteins, a proline-rich domain containing Homer and Cortactin binding regions, and a C-terminal SAM domain (Naisbitt et al., 1999). Shank3 has been suggested to act as a master organizer of the PSD because of its ability to interact with multiple key synaptic components including glutamate receptor complexes, anchoring proteins, and actin cytoskeleton (Sheng and Kim, 2000; Hayashi et al., 2009). However, the molecular targets of Shank3 causally linked to the ASD-like behavioral deficits are largely unknown.

The NMDA-type glutamate receptor, a key PSD protein controlling neural development and synaptic plasticity underlying cognitive processes, is physically associated with Shank3 (Naisbitt et al., 1999; Ehlers, 1999). Recent evidence has implicated NMDA receptor (NMDAR) dysfunction in ASD (Carlson, 2012). Administration of NMDAR antagonists or NR1 deficiency induces ASD-like social deficits in mice (Zou et al., 2008). *Shank2* or *Shank3*-lacking mice exhibit impaired NMDAR-dependent synaptic plasticity along with ASD-related behaviors (Wang et al., 2011; Won et al., 2012; Kouser et al., 2013).

The NMDAR is closely tied to actin filaments through actin-binding proteins (Wyszynski et al., 1997). The integrity of actin cytoskeleton is critical for NMDAR membrane delivery and stability (Rosenmund and Westbrook, 1993; Allison et al., 1998), as well as the plasticity of NMDAR-mediated synaptic responses (Morishita et al., 2005). Shank3 is found to be located at the tip of actin filaments and enhances its polymerization (Durand et al., 2012), and Shank overexpression induces spine enlargement in spiny excitatory neurons (Sala et al., 2001). In vivo Shank3 interactome analysis has identified several actin regulators that bind to Shank3 (Han et al., 2013). Thus, it is conceivable that Shank3 deficiency may disrupt actin dynamics, leading to NMDAR hypofunction, which contributes to the ASD symptoms.

A key player in the regulation of actin dynamics is Rac1, a member of the family of Rho GTPases, which acts as a molecular switch in intracellular signaling pathways. The activity of the GTPases is regulated by guanine nucleotide exchange factors (GEFs). Rac1 stimulates spine formation, dendrite initiation, elongation, and branching complexity (Threadgill et al., 1997; Ridley, 2006). The major downstream effectors of Rac1 are p21-activated kinase (PAK) and LIM-domain containing protein

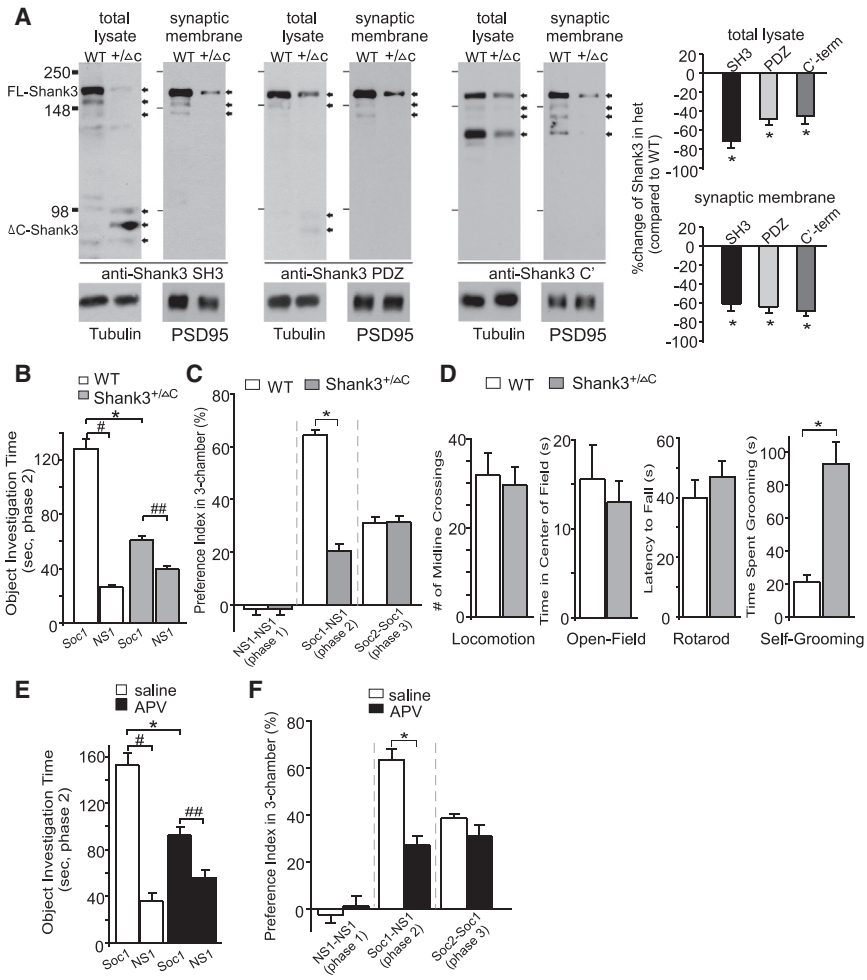

Figure 1. *Shank3*-Deficient Mice Exhibit Social Deficits and Repetitive Behaviors

(A) Western blots and bar graphs (mean ± SEM) showing the loss of endogenous full-length Shank3 (FL-Shank3) isoforms in the total cortical lysates and postsynaptic density (PSD) fraction of frontal cortex from heterozygous mice expressing C-terminal deleted Shank3, Shank3$^{+/\Delta C}$. Antibodies against Shank3 SH3 domain, PDZ domain, or C-term were used. *p < 0.001, t test.

(B) Bar graphs (mean ± SEM) showing the time spent investigating either the social (Soc1) or nonsocial (NS1) stimulus in sociability testing (phase 2) in male wild-type (WT) versus Shank3$^{+/\Delta C}$ mice. *p < 0.001, WT versus Shank3$^{+/\Delta C}$; #p < 0.001, ##p < 0.01, Soc1 versus NS1, two-way ANOVA.

(C) Bar graphs (mean ± SEM) showing the preference index for investigating different stimuli at three phases of sociability testing in WT versus Shank3$^{+/\Delta C}$ mice. *p < 0.001, t test.

(D) Bar graphs (mean ± SEM) showing the number of midline crossing in locomotion tests, the time spent in the center during open-field tests, the latency to fall during rotarod tests, and the time spent self-grooming in WT versus Shank3$^{+/\Delta C}$ mice. *p < 0.01, t test.

(E) Bar graphs (mean ± SEM) showing the time spent investigating either the Soc1 or NS1 stimulus in sociability testing (phase 2) in WT mice receiving a PFC injection of either saline or APV (1 mM, 1 μl each side). *p < 0.001, saline versus APV; #p < 0.001, ##p < 0.01, Soc1 versus NS1, two-way ANOVA.

(F) Bar graphs (mean ± SEM) showing the preference index for investigating different stimuli at three phases of sociability testing in WT mice receiving a PFC injection of either saline or APV. *p < 0.01, t test.

See also Figure S1 and Movies S1, S2, and S3.

kinase (LIMK), which facilitate actin filament assembly through the phosphorylation and inactivation of cofilin (Sells et al., 1997; Arber et al., 1998), a major actin depolymerizing factor (Bamburg 1999; dos Remedios et al., 2003). Aberrant Rac1/PAK/LIMK signaling could lead to abnormal neuronal connectivity and synaptic plasticity, as well as deficient cognitive and emotional functioning (Hayashi et al., 2004; Golden et al., 2013). Importantly, genetic analyses have revealed that intellectual disability (Ramakers, 2002), autism (Gilman et al., 2011), and schizophrenia (Fromer et al., 2014) all have enriched mutations in genes regulating actin filament network at glutamatergic synapses, indicating that actin dysregulation is one common pathophysiological mechanism for these disorders.

Our recent studies found that Shank3 knockdown in vitro led to the reduced NMDAR function in cortical neurons via an actin-dependent mechanism (Duffney et al., 2013). In the current study, we examined whether the NMDAR hypofunction and ASD-like behavioral deficits in autism models with *Shank3* haploinsufficiency are caused by the decreased Rac1/PAK signaling and increased actin depolymerization by cofilin, and whether manipulating actin regulators could rescue the synaptic and behavioral deficiencies in this autism model.

RESULTS

Shank3-Deficient Mice Exhibit ASD-like Behaviors and Impaired NMDAR Function in Prefrontal Cortex

To determine the impact of Shank3 deficiency on autism-like behaviors, we used heterozygous mice with C-terminal deleted Shank3 (deletion of exon 21, which includes the Homer- and Cortactin-binding domains), Shank3$^{+/\Delta C}$, since hemizygous mutation in the *Shank3* gene has been linked to autism and intellectual disability (Bonaglia et al., 2001; Durand et al., 2007). Using antibodies against Shank3 SH3 domain, PDZ domain, or C-term (Figure 1A), we found that, compared to wild-type mice, Shank3$^{+/\Delta C}$ mice showed a significant knockdown of the endogenous full-length Shank3 (FL-Shank3) isoforms (~190 kDa) in total and synaptosomal fraction of frontal cortical lysates (50%–70% reduction, n = 7 pairs, p < 0.001, t test), hence providing an excellent model for studying the impact of the loss of naturally occurring Shank3 proteins. Interestingly, the C-term deleted Shank3 protein (ΔC-Shank3, ~90 kDa) can only be found in total brain lysates, but not the synaptosomal fraction, suggesting that ΔC-Shank3 has lost its synaptic distribution, probably due to the lack of its binding to Cortactin/F-actin.

Homozygous Shank3$^{\Delta C/\Delta C}$ mice had an even more prominent loss of endogenous FL-Shank3 isoforms detected with the three Shank3 antibodies (~85% reduction, n = 4 pairs, Figure S1A).

Juvenile male Shank3$^{+/\Delta C}$ mice and age-matched wild-type mice were subject to the three-chamber social interaction assay (Wang et al., 2011; Won et al., 2012). Briefly, the test is composed of three phases with various stimuli placed in each of two side chambers. Phase 1 contains two identical nonsocial stimuli (NS1 and NS1), phase 2 contains a nonsocial stimulus (NS1) and a social stimulus (Soc1), and phase 3 contains a known social stimulus (Soc1) and a novel social stimulus (Soc2). The preference index for one stimulus over the other stimulus in each phase was compared.

As shown in Figure 1B, during the presentation of both a social and a non-social stimuli (Soc1-NS1, phase 2), wild-type mice spent significantly more time exploring the social stimulus over the non-social object, while Shank3$^{+/\Delta C}$ mice showed a significant loss of the preference for the social stimulus (WT social: 126.1 ± 6.8 s, WT nonsocial: 26.4 ± 1.6 s, n = 52; Shank3$^{+/\Delta C}$ social: 60.6 ± 3.0 s, Shank3$^{+/\Delta C}$ nonsocial: 39.5 ± 1.8 s, n = 52, $F_{1,204\ (interaction)} = 100.8$, $p < 0.001$, two-way ANOVA; see Movies S1 and S2). The significantly reduced social preference index in *Shank3*-deficient mice (Figure 1C, WT: 64.3% ± 1.9%, n = 52; Shank3$^{+/\Delta C}$: 20.7% ± 2.5%, n = 52, $p < 0.001$, t test) suggests an impairment of sociability. The social deficits in young male Shank3$^{+/\Delta C}$ mice were so evident that it led to 100% accuracy in blind tests (i.e., where raters had no prior knowledge about the genotypes). When presented with two identical non-social stimuli (NS1-NS1, phase 1), no preference was observed in either genotype (Figure 1C, WT: −1.3% ± 2.5%, n = 45; Shank3$^{+/\Delta C}$: −1.6% ± 2.1%, n = 45, $p > 0.05$, t test). When exposed to two social stimuli (Soc2-Soc1, phase 3), both genotypes displayed similar preference for the novel over the familiar social stimulus (Figure 1C, WT: 31.1% ± 2.3%, n = 46; Shank3$^{+/\Delta C}$: 31.6% ± 2.3%, n = 49, $p > 0.05$, t test), suggesting that *Shank3*-deficient mice have intact social novelty recognition memory. Consistently, the impaired sociability (phase 2) in Shank3$^{+/\Delta C}$ mice was not due to deficits in novelty recognition, because when animals were exposed to a social and a "novel" non-social stimuli (Soc1-NS2) in phase 2, a similar difference on the preference index for the social stimulus over the non-social stimulus was found between the two genotypes (WT: 56.1% ± 5.3%, n = 10; Shank3$^{+/\Delta C}$: 16.1% ± 5.8%, n = 12, $p < 0.001$, t test).

Homozygous Shank3$^{\Delta C/\Delta C}$ mice (juvenile male) also exhibited significantly lower social preference (Soc1-NS1, phase 2) in the three-chamber sociability tests (Figure S1B, WT: 59.7% ± 2.0%, n = 12; Shank3$^{\Delta C/\Delta C}$: 24.2% ± 8.1%, n = 10, $p < 0.001$, t test). Among the large number of animals we examined, the majority of Shank3$^{+/\Delta C}$ or Shank3$^{\Delta C/\Delta C}$ mice exhibited deficits in the social preference, comparing to wild-type counterparts (Figure S1C). Moreover, Shank3$^{\Delta C/\Delta C}$ mice had dramatically reduced investigation time toward both social stimuli in phase 3 (Figure S1D, WT: 130.7 ± 8.0 s, n = 21; Shank3$^{+/\Delta C}$: 92.8 ± 9.4 s, n = 21; Shank3$^{\Delta C/\Delta C}$: 29.1 ± 6.0 s, n = 10, $F_{2,49} = 25.7$, $p < 0.001$, ANOVA), indicating that they have either a social avoidance phenotype or less social drive.

Wild-type and *Shank3*-deficient mice were also compared in other behavioral tasks (Figure 1D). No differences were seen in locomotion (midline crossing #, WT: 31.9 ± 5.0, n = 7, Shank3$^{+/\Delta C}$: 29.6 ± 5.0, n = 9, $p > 0.05$, t test). Both genotypes showed similar results in the open-field test (time in center, WT: 15.5 ± 3.8 s, n = 11, Shank3$^{+/\Delta C}$: 13.0 ± 2.4 s, n = 11, $p > 0.05$, t test) and the rotarod test (latency to fall, WT: 40.0 ± 6.1 s, n = 12; Shank3$^{+/\Delta C}$: 47.1 ± 5.3 s, n = 14, $p > 0.05$, t test), suggesting that anxiety level and motor coordination are normal in *Shank3*-deficient mice. However, differences were evident in self-grooming, with *Shank3*-deficient mice spending significantly more time engaged in this repetitive behavior (WT: 21.4 ± 4.4 s, n = 25, Shank3$^{+/\Delta C}$: 93.1 ± 13.3 s, n = 22, $p < 0.01$, t test, see Movie S3).

To identify the cellular and molecular basis for the social interaction behavior, we focused on prefrontal cortex (PFC), a brain region controlling high-level executive functions, which has been suggested as a key area mediating ASD-like behaviors (Anderson et al., 1999; Hill, 2004). Given the data implicating NMDAR dysfunction in ASD (Carlson, 2012), we blocked NMDA receptors in PFC of wild-type mice and examined their social interaction behavior. To do this, the NMDAR antagonist APV was stereotaxically injected bilaterally into prelimbic regions. As shown in Figure 1E, compared to saline-injected mice, mice injected with APV displayed a significant decrease of the preference for the social stimulus over the non-social object in phase 2 of the three-chamber social interaction assay (saline, social: 152.7 ± 10.0 s, nonsocial: 36.0 ± 6.9 s, n = 6; APV, social: 92.3 ± 7.0 s, nonsocial: 56.0 ± 6.5 s, n = 6, $F_{1,20\ (interaction)} = 27.0$, $p < 0.0001$, two-way ANOVA). The significant reduction of social preference index in phase 2 by APV injection (Figure 1F, saline: 63.4% ± 4.4%, n = 6; APV: 27.0% ± 3.9%, n = 6, $p < 0.01$, t test) suggests that NMDA receptors in PFC are crucial for sociability.

Next, we examined NMDAR function in PFC of *Shank3*-deficient mice, alterations of which may underlie the ASD-like social deficits in these animals. Layer 5 PFC pyramidal neurons, which showed the clearest deficits in autistic children (Stoner et al., 2014), were selected for the recording of NMDAR-mediated excitatory postsynaptic currents (EPSCs). As shown in Figure 2A, NMDAR-EPSC induced by a series of stimulus intensities was markedly reduced in Shank3$^{+/\Delta C}$ mice (30%–40% decrease, WT: n = 26, Shank3$^{+/\Delta C}$: n = 37). Two-way ANOVA analysis revealed a significant main effect of genotype ($F_{1,305} = 118.4$, $p < 0.001$) and stimulation intensity ($F_{4,305} = 26.6$, $p < 0.001$). Post hoc multiple comparison tests revealed that PFC neurons from Shank3$^{+/\Delta C}$ had significantly lower NMDAR responses than those from WT mice ($p < 0.01$). In contrast, AMPAR-EPSC was largely unchanged in PFC pyramidal neurons from *Shank3*-deficient mice (Figure 2B, <5% decrease, WT: n = 18, Shank3$^{+/\Delta C}$: n = 19, $F_{1,175\ (genotype)} = 1.5$, $p > 0.05$, two-way ANOVA). The NMDAR- to AMPAR-EPSC ratio was significantly smaller in PFC pyramidal neurons from *Shank3*-deficient mice than those from age-matched wild-type mice (Figure 2C, WT: 0.71 ± 0.05, n = 12, Shank3$^{+/\Delta C}$: 0.52 ± 0.04, n = 14; $p < 0.01$, t test). A smaller but significant reduction of NMDAR-EPSC was also observed in hippocampal CA1 pyramidal neurons of

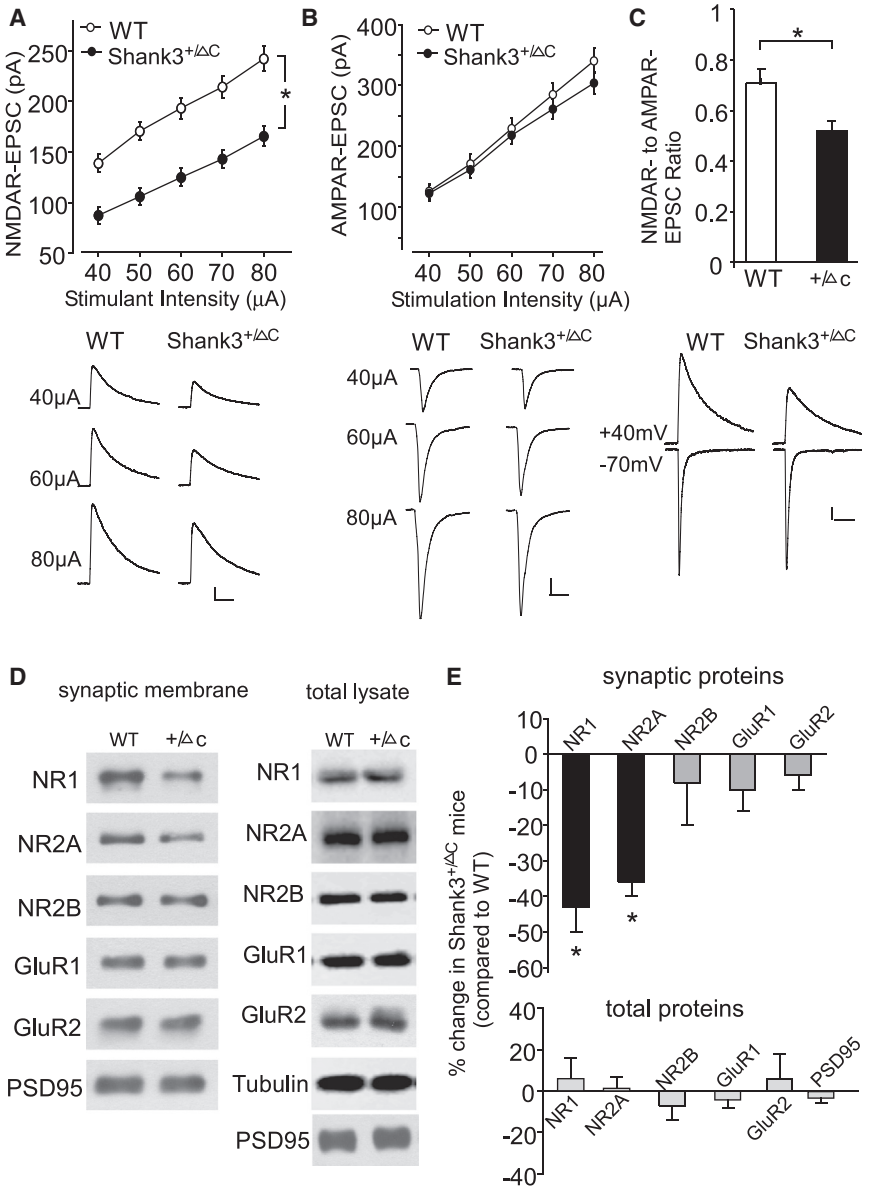

Figure 2. *Shank3*-Deficient Mice Show the Diminished NMDAR Synaptic Function and Synaptic Distribution in Prefrontal Cortex

(A and B) Input-output curves (mean ± SEM) of NMDAR-EPSC (A) and AMPAR-EPSC (B) in response to a series of stimulation intensities in PFC pyramidal neurons from male WT versus Shank3$^{+/\Delta C}$ mice. *p < 0.01, ANOVA. Inset: representative EPSC traces at different stimuli. Scale bars, 40 pA, 100 ms (NMDA); 50 pA, 25 ms (AMPA).

(C) Bar graphs (mean ± SEM) of the NMDAR- to AMPAR-EPSC ratio in WT versus Shank3$^{+/\Delta C}$ mice. *p < 0.01, t test. Inset: representative traces of NMDAR-EPSC and AMPAR-EPSC recorded in the same PFC pyramidal neurons from WT versus Shank3$^{+/\Delta C}$ mice. Scale bar, 20 pA, 100 ms.

(D) Immunoblots showing the expression of NMDAR and AMPAR subunits in the Triton-insoluble synaptosomal fraction or the total lysate of frontal cortical slices from WT versus Shank3$^{+/\Delta C}$ mice.

(E) Quantification (mean ± SEM) of the alteration of synaptosomal (normalized to PSD-95) and total (normalized to Tubulin) glutamate receptors in Shank3$^{+/\Delta C}$ mice, compared to WT mice. *p < 0.01, WT versus Shank3$^{+/\Delta C}$, t test.

See also Figures S2 and S3.

Shank3$^{+/\Delta C}$ mice (Figure S2A, WT: n = 19, Shank3$^{+/\Delta C}$: n = 17, $F_{1,170\ (genotype)}$ = 19.1, p < 0.05, two-way ANOVA). No significant loss of NMDAR-EPSC was found in dorsal striatal medium spiny neurons of Shank3$^{+/\Delta C}$ mice (Figure S3A, <5% decrease, WT: n = 13, Shank3$^{+/\Delta C}$: n = 15, $F_{1,130\ (genotype)}$ = 0.5, p > 0.05, two-way ANOVA). These data indicate that *Shank3* deficiency causes prominent NMDAR hypofunction in the PFC in vivo, consistent with our findings in cortical cultures with Shank3 knockdown (Duffney et al., 2013).

The selective loss of cortical NMDAR function in *Shank3*-deficient mice could result from the reduced number of NMDA receptors at synapses. To test this, we compared subcellular distribution of glutamate receptors in PFC of wild-type and *Shank3*-deficient mice. As shown in Figures 2D and 2E, NR1 and NR2A subunits in the Triton-insoluble synaptosome fraction of frontal cortical tissues were significantly reduced in Shank3$^{+/\Delta C}$ mice (NR1: 43% ± 7% decrease, NR2A: 36% ± 4% decrease, n = 6 pairs, p < 0.01, t test), while synaptosomal NR2B, GluR1, and GluR2 subunits were largely unchanged (n = 6 pairs, p > 0.05, t test). No significant changes were found on the total levels of NR1, NR2A, NR2B, GluR1, and GluR2 subunits in PFC of Shank3$^{+/\Delta C}$ mice (n = 14 pairs, p > 0.05, t test). The reduced amount of NMDARs in the synaptic pools suggests the loss of NMDAR delivery to the plasma membrane of PSDs in *Shank3*-deficient conditions.

Shank3-Deficient Mice Exhibit Altered Rac1/PAK/Cofilin Signaling and Dysregulated F-actin in Frontal Cortex

Given the importance of Rac1 signaling and actin stability in Shank3-regulated NMDAR membrane trafficking (Duffney et al., 2013), we next examined whether actin regulators were altered in *Shank3*-deficient mice. It has been shown that βPIX, the guanine nucleotide exchange factor (GEF) for Rac1 that promotes functional coupling of Rac1 and PAK (Manser et al., 1998), interacts with Shank at excitatory synaptic sites (Park et al., 2003). In the total lysates from prefrontal cortical slices of Shank3$^{+/\Delta C}$ mice (Figures 3A and 3B), the protein level of βPIX

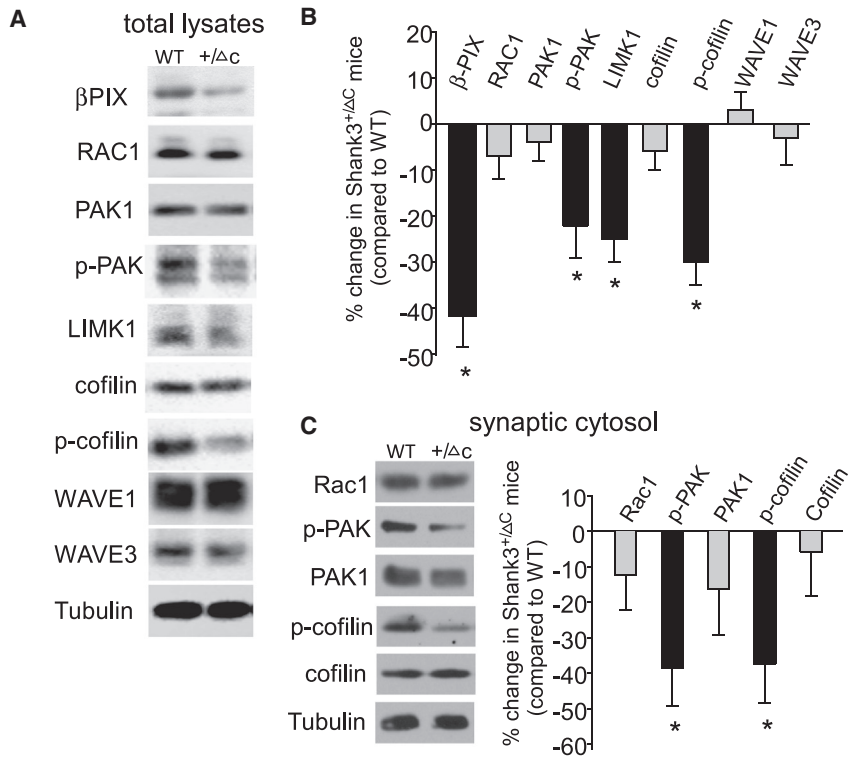

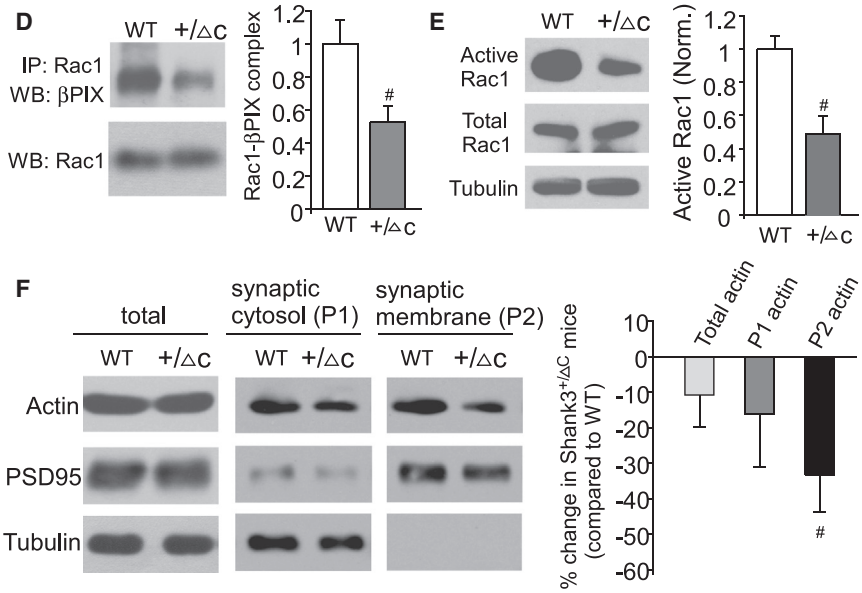

Figure 3. *Shank3*-Deficient Mice Exhibit Decreased Rac1/PAK Signaling, Increased Cofilin Activity, and Reduced Synaptic F-actin in Prefrontal Cortex

(A) Immunoblots showing the expression of actin regulators, such as βPIX (the GEF involved in Rac1 activation), Rac1, PAK1, p-PAK (active PAK1/2/3), LIMK1, cofilin, p-cofilin (inactive cofilin), WAVE1, and WAVE3 in total lysates from PFC of WT versus Shank3$^{+/\Delta C}$ mice.

(B) Quantification (mean ± SEM) of the alteration of actin regulators in Shank3$^{+/\Delta C}$ mice. *p < 0.01, WT versus Shank3$^{+/\Delta C}$, t test.

(C) Immunoblots and quantification (mean ± SEM) showing the alteration of actin regulators in the cytosolic fraction of synapses from PFC of Shank3$^{+/\Delta C}$ mice. *p < 0.01, WT versus Shank3$^{+/\Delta C}$, t test.

(D and E) Representative blots and quantification (mean ± SEM) showing the active Rac1 (D: βPIX-bound, E: GST-PBD pull-down) and total Rac1 in WT versus Shank3$^{+/\Delta C}$ mice. PBD, PAK1 protein-binding domain. #p < 0.05, t test.

(F) Immunoblots and quantification (mean ± SEM) showing actin in the Triton-soluble synaptic cytosolic fraction (G-actin) versus Triton-insoluble synaptic membrane fraction (F-actin) from PFC of WT versus Shank3$^{+/\Delta C}$ mice. #p < 0.05, t test.

See also Figure S4.

was significantly decreased (41.6% ± 7.0% decrease, n = 9 pairs, p < 0.01, t test), suggesting reduced Rac1 activity. Moreover, the downstream effectors of the Rac1 signaling cascade, such as activated (Thr423/Thr402/Thr421-phosphorylated) PAK1/2/3 and LIMK were significantly reduced in Shank3$^{+/\Delta C}$ mice (p-PAK: 22% ± 7% decrease, n = 17 pairs; LIMK: 25% ± 5% decrease, n = 11 pairs, p < 0.01, t test). A key downstream target of PAK/LIMK signaling is cofilin, the major actin depolymerizing factor (Bamburg, 1999), which is inactivated by phosphorylation at Ser3 (dos Remedios et al., 2003). Shank3$^{+/\Delta C}$ mice had the unchanged total cofilin (n = 13 pairs, p > 0.05, t test), but a significantly decreased level of the inactive (Ser3-phosophorylated) form of cofilin (p-cofilin: 30% ± 5% decrease, n = 13 pairs, p < 0.01, t test), indicating that the active form of cofilin is elevated in the cortex of *Shank3*-deficient mice.

Given that Shank3 directly interacts with the Arp2/3 complex to increase F-actin levels in transgenic mice overexpressing Shank3 (Han et al., 2013), we also examined the Arp2/3 activator WAVE1/3, which is involved in actin filament assembly. As shown in Figures 3A and 3B, no significant differences were found in the expression of WAVE1 (n = 16 pairs, p > 0.05, t test) or WAVE3 (n = 9 pairs, p > 0.05, t test) in cortical lysates from Shank3$^{+/\Delta C}$ mice.

We then examined the alteration of actin regulators in the cytosolic fraction of synapses from PFC of Shank3$^{+/\Delta C}$ mice. As shown in Figure 3C, the levels of synaptic p-PAK (active) and p-cofilin (inactive) were significantly reduced (p-PAK: 38.6% ± 10.5% decrease, n = 8 pairs, p < 0.01, t test, p-cofilin: 37.3% ± 11.0% decrease, n = 5 pairs, p < 0.01, t test), indicating

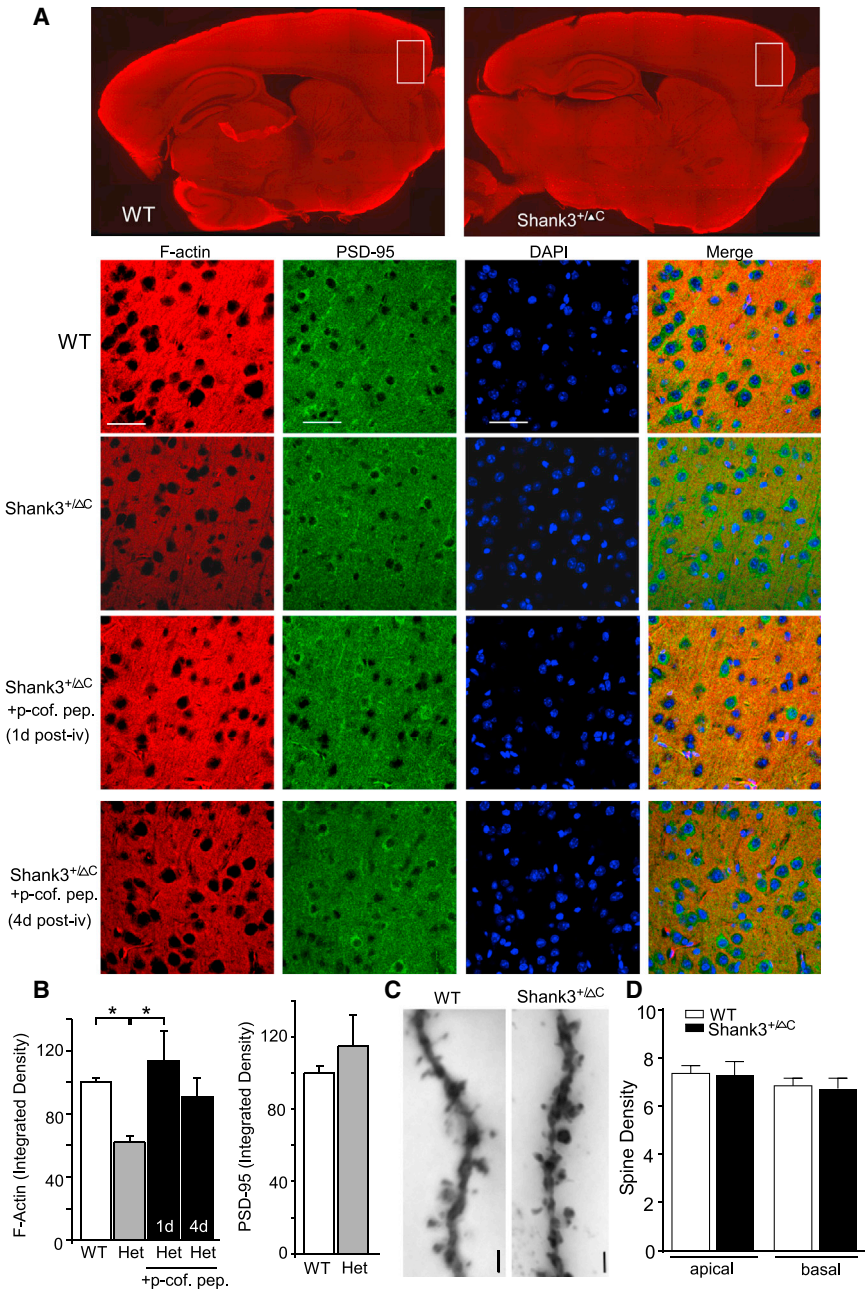

Figure 4. *Shank3*-Deficient Mice Have the Reduced F-actin Level in Prefrontal Cortex, Which Is Restored by Inhibition of Cofilin

(A) High-magnification confocal images (40×) of F-actin staining with phalloidin (co-stained with PSD-95 and DAPI) in PFC slices of WT versus Shank3$^{+/\Delta C}$ mice without or with an i.v. injection of the brain-permeable cofilin inhibitory peptide, TAT-p-cofilin peptide (15 pmol/g). Scale bars, 50 μm. Shown at the top are low-magnification (5×) images of F-actin staining in semi-sagittal slices of WT versus Shank3$^{+/\Delta C}$ mice.

(B) Quantification (mean ± SEM) of F-actin and PSD-95 levels (integrated densities) in PFC slices of different animal groups. *p < 0.01, one-way ANOVA.

(C) Representative images of Golgi-stained apical dendrites in PFC pyramidal neurons from WT and Shank3$^{+/\Delta C}$ mice. Scale bar, 2 μm.

(D) Quantification (mean ± SEM) of apical and basal dendritic spine densities in PFC neurons from WT versus Shank3$^{+/\Delta C}$ mice.

See also Figures S2 and S3.

that PAK/cofilin signaling is aberrant in the synapses of PFC neurons from *Shank3*-deficient mice.

Next, we examined whether the activity of Rac1, which is upstream of PAK/cofilin signaling, is altered in PFC of Shank3$^{+/\Delta C}$ mice. Cell line studies have found that βPIX specifically binds the C-term of Rac1, but not of Cdc42 or RhoA, and the interaction with βPIX is required for the membrane targeting and localized activation of Rac1 (ten Klooster et al., 2006), so we performed co-immunoprecipitation experiments to examine βPIX-bound (active) Rac1 in PFC slices. As shown in Figure 3D, the Rac1-βPIX complex was significantly decreased in Shank3$^{+/\Delta C}$ mice (46% ± 10% decrease, n = 7 pairs, p < 0.05, t test), suggesting that Rac1 activity is decreased by Shank3 deficiency.

To further measure active Rac1 directly, we performed pull-down assay using the purified GST-PAK1 protein-binding domain (PBD) that specifically interacts with GTP-bound Rac1 GTPase. As shown in Figure 3E, compared to wild-type counterparts, the level of active Rac1 was significantly lower in PFC of Shank3$^{+/\Delta C}$ mice (51% ± 11% decrease, n = 4 pairs, p < 0.05, t test).

The increased active cofilin may lead to the alteration of actin filaments in Shank3$^{+/\Delta C}$ mice, so we compared the Triton-soluble monomeric actin (G-actin) and the Triton-insoluble filamentous polymerized actin (F-actin) in the synaptic fraction of frontal cortex from WT versus Shank3$^{+/\Delta C}$ mice, using the approach similar to what was previously described (Fukazawa et al., 2003). We found that the level of total actin or actin at the synaptic cytosol (soluble) was largely unchanged, but the level of synaptic F-actin (insoluble) in PFC of *Shank3*-deficient mice was significantly lower, compared to WT counterparts (Figure 3F, 33.1% ± 10.4% decrease, n = 6 pairs, p < 0.05, t test).

To more directly visualize F-actin, we performed immunostaining with phalloidin. As shown in Figures 4A and 4B, *Shank3*-deficient mice had a significant decrease of F-actin expression in PFC slices (integrated density, WT: 100 ± 2.9, n = 9 mice/54 images; Shank3$^{+/\Delta C}$: 62.1 ± 3.9, n = 8 mice/49 images, p < 0.01, ANOVA). In contrast to the reduced F-actin level, Shank3$^{+/\Delta C}$

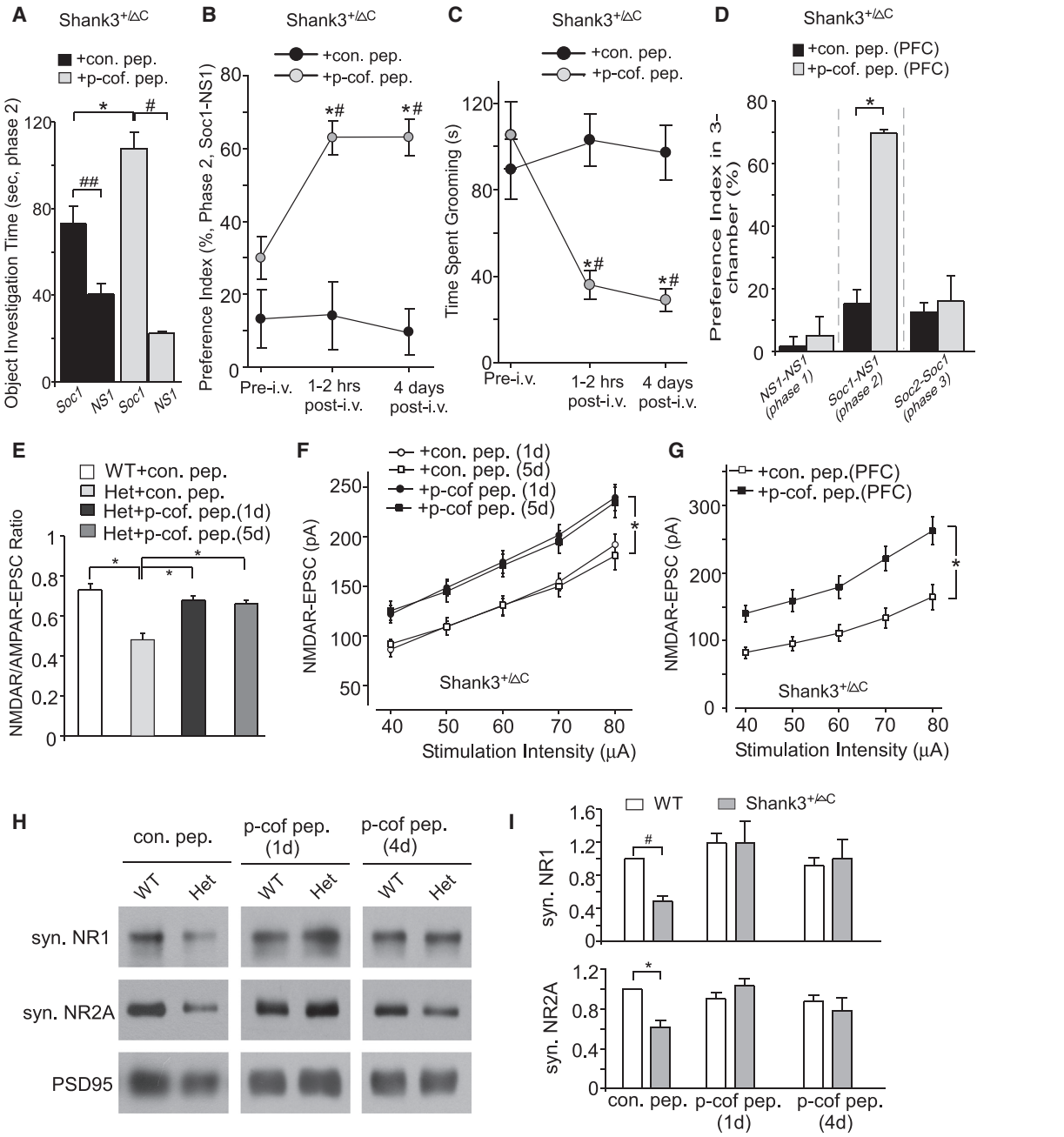

Figure 5. Inhibition of Cofilin Rescues ASD-like Behaviors and Restores NMDAR Function in *Shank3*-Deficient Mice

(A) Bar graphs (mean ± SEM) showing the time spent investigating either the social (Soc1) or nonsocial (NS1) stimulus during phase 2 of sociability testing in Shank3$^{+/\Delta C}$ mice with an i.v. injection of TAT-p-cofilin peptide or TAT control peptide (15 pmol/g). *p < 0.01, control versus p-cofilin peptide; #p < 0.001, ##p < 0.01, Soc1 versus NS1, two-way ANOVA.

(B) Plots (mean ± SEM) of social preference index (phase 2) in Shank3$^{+/\Delta C}$ mice with an i.v. injection of TAT-p-cofilin peptide or TAT control peptide at different time points. *p < 0.001, control versus p-cofilin peptide; #p < 0.001, pre- versus post-injection, two-way rmANOVA.

(C) Plots (mean ± SEM) of the time engaged in self-grooming behavior in Shank3$^{+/\Delta C}$ mice with an i.v. injection of TAT-p-cofilin peptide or TAT control peptide at different time points. *p < 0.05, control versus p-cofilin peptide; #p < 0.001, pre- versus post-injection, two-way rmANOVA.

(D) Bar graphs (mean ± SEM) showing the preference index for investigating different stimuli at three phases of sociability testing in Shank3$^{+/\Delta C}$ mice with a local (PFC) injection of TAT-p-cofilin peptide (5 μM, 1 μl per side) or TAT control peptide. *p < 0.01, t test.

(E and F) Bar graphs (mean ± SEM) of the NMDAR- to AMPAR-EPSC ratio (E) and input-output curves (mean ± SEM) of NMDAR-EPSC (F) in PFC pyramidal neurons from WT versus Shank3$^{+/\Delta C}$ mice receiving a systemic injection of TAT-p-cofilin peptide or TAT control peptide (15 pmol/g, i.v.). Recordings were performed at 1 or 5 days post-injection. *p < 0.01, one-way ANOVA (E). *p < 0.05, two-way ANOVA (F).

(legend continued on next page)

mice had normal PSD-95 expression in PFC (WT: 100 ± 4.2, n = 4 mice/35 images; Shank3$^{+/\Delta C}$: 112.9 ± 17.1, n = 4 mice/36 images; p > 0.05, t test), suggesting that the number of synapses was intact. Hippocampal slices from Shank3$^{+/\Delta C}$ mice also exhibited a smaller but significant reduction of F-actin (Figure S2B, WT: 100 ± 2.2, n = 10 mice/43 images; Shank3$^{+/\Delta C}$: 78.6 ± 5.6, n = 7 mice/26 images, p < 0.01, t test). No significant alteration of F-actin was observed in dorsal striatal slices from Shank3$^{+/\Delta C}$ mice (Figure S3B, WT: 100 ± 2.9, n = 6 mice/34 images; Shank3$^{+/\Delta C}$: 100 ± 5.9, n = 5 mice/26 images, p > 0.05, t test), which may be due to the lack of changes in βPIX expression in the striatum of Shank3$^{+/\Delta C}$ mice (Figure S3C, n = 5 pairs, p > 0.05, t test). These data suggest that *Shank3* deficiency mainly causes a cortical region-specific loss of actin filaments.

To restore cortical actin filaments, we used a peptide consisting of one to 16 residues of Ser3-phosphorylated cofilin as an inhibitor of endogenous cofilin (Morishita et al., 2005). The p-cofilin peptide was coupled to the protein transduction domain of the HIV TAT protein to render it cell permeable. Since systemic injections can reliably deliver TAT peptides into CNS neurons (Aarts et al., 2002; Borsello et al., 2003), we gave Shank3$^{+/\Delta C}$ mice an intravenous (i.v.) injection of TAT-p-cofilin peptide (15 pmol/g). As shown in Figures 4A and 4B, F-actin in Shank3$^{+/\Delta C}$ mice was increased to the normal level after a single injection of the cofilin inhibitory peptide (113.7 ± 18.8, n = 5 mice/32 images, p < 0.01, ANOVA, compared to Shank3$^{+/\Delta C}$) and remained elevated even at 4 days post-injection (90.7 ± 12.3, n = 7 mice/55 images). Taken together, these data indicate that Shank3 deficiency leads to increased cofilin activity and actin depolymerization, which may contribute to the impaired NMDAR trafficking and ASD-like behavioral deficits.

To test whether the number of synapses was altered in Shank3$^{+/\Delta C}$ mice, Golgi staining was performed to examine dendritic spines on PFC pyramidal neurons from WT versus Shank3$^{+/\Delta C}$ mice. No significant changes were observed in the spine densities (# of spines/10 μm) on apical or basal dendrites (Figures 4C and 4D, apical, WT: 7.37 ± 0.33, Shank3$^{+/\Delta C}$: 7.30 ± 0.57; basal, WT: 6.85 ± 0.32, Shank3$^{+/\Delta C}$: 6.74 ± 0.42, n = 15–20 neurons/three pairs of mice, p > 0.05, t test), indicating that the reduced F-actin in frontal cortex of *Shank3*-deficient mice did not lead to an obvious loss of synapses.

In addition, we examined whether changes in actin signaling can be found in an independent *Shank3*-deficient mouse line. Mice with a targeted disruption of Shank3 exons coding for the N-terminal ankyrin repeat domain, which leads to the loss of the longest isoforms of Shank3 (*Shank3*-KO; Bozdagi et al., 2010), were used. We carried out unbiased analyses using two-dimensional fluorescence difference gel electrophoresis (2D-DIGE). Triplicate comparisons identified several spots showing differential expression between cortical PSD fractions from WT and *Shank3*-KO, including actin-binding proteins (Figure S4A). To validate the finding in an independent cohort, immunoblot analyses were performed in PSD fractions from additional WT and *Shank3*-KO mice. As shown in Figure S4B, *Shank3*-KO mice had a significant reduction of ^{Ser3}p-cofilin (inactive cofilin, 60% ± 2.7% decrease, n = 4 pairs, p < 0.01, t test) and LIMK1 (a kinase responsible for cofilin phosphorylation and inactivation, 35% ± 4.8% decrease, n = 4 pairs, p < 0.01, t test), consistent with our findings in Shank3$^{+/\Delta C}$ mice.

Inhibiting Cofilin to Stabilize F-actin Rescues Behavioral Deficits and Restores NMDAR Function in Shank3-Deficient Mice

Since male Shank3$^{+/\Delta C}$ mice have a prominent reduction of cortical actin filaments, which can be rescued by the TAT-p-cofilin peptide (Figure 4), we further examined whether the ASD-like behavioral deficits in these mice could be rescued by cofilin inhibition. Behavioral tests found that after the i.v. injection of TAT-p-cofilin peptide (15 pmol/g), but not TAT control peptide, *Shank3*-deficient mice displayed a significant increase in the preference of exploring the social stimulus over the non-social object in phase 2 of sociability tests (Figure 5A, p-cofilin peptide, social: 107.6 ± 7.5 s, nonsocial: 22.4 ± 0.9 s, n = 9; TAT control peptide, social: 73.0 ± 8.2 s, nonsocial: 40.5 ± 4.8 s, n = 11; $F_{1,36\ (interaction)}$ = 17.5, p < 0.01, two-way ANOVA). The significantly increased social preference index (Soc1-NS1, phase 2) in Shank3$^{+/\Delta C}$ mice induced by the p-cofilin peptide (Figure 5B, p-cofilin peptide, pre-injection: 31.7% ± 3.9%, 1–2 hr post-injection: 62.1% ± 2.8%, 4 days post-injection: 62.7% ± 3.1%, n = 12; TAT control peptide, pre-injection: 21.5% ± 1.8%, 1–2 hr post-injection: 20.5% ± 5.4%, 4 days post-injection: 13.6% ± 2.9%, n = 8; $F_{2,36\ (interaction)}$ = 13.8, p < 0.0001, two-way repeated-measure ANOVA [rmANOVA]) demonstrated a restoration of sociability with cofilin inhibition. The fast and long-lasting rescue of social deficits can be clearly seen in Movies S4, S5, and S6. The peptide injection did not cause any significant changes in non-social (NS1-NS1, phase 1) or novel social (Soc2- Soc1, phase 3) tests at any time point (data not shown).

To test the effectiveness of cofilin inhibition in rescuing other ASD-like behaviors, we examined self-grooming in *Shank3*-deficient mice. As shown in Figure 5C, Shank3$^{+/\Delta C}$ mice injected (i.v.) with TAT-p-cofilin peptide, but not TAT control peptide, had a significant decrease in self-grooming time (p-cofilin peptide, pre-injection: 105.3 ± 15.6 s, 1–2 hr post-injection: 36.0 ± 6.4 s, 4 days post-injection: 29.0 ± 5.3 s, n = 8; control peptide, pre-injection: 89.4 ± 14.0 s, 1–2 hr post-injection: 103.0 ± 12.1 s, 4 days post-injection: 97.1 ± 12.6 s, n = 8; $F_{2,28\ (interaction)}$ = 19.8, p < 0.0001, two-way rmANOVA, see Movie S7).

We further performed the bilateral stereotaxic injection of the cofilin inhibitory peptide into prelimbic regions of *Shank3*-deficient mice and examined sociability rescue. Shank3$^{+/\Delta C}$ mice

(G) Input-output curves (mean ± SEM) of NMDAR-EPSC in PFC pyramidal neurons from WT versus Shank3$^{+/\Delta C}$ mice with a local injection of TAT-p-cofilin peptide or TAT control peptide to PFC. *p < 0.01, ANOVA.

(H and I) Immunoblots and quantification (mean ± SEM) of the expression of NR1 and NR2A in the Triton-insoluble synaptosomal fraction of frontal cortical tissues from WT versus Shank3$^{+/\Delta C}$ mice injected with TAT-p-cofilin peptide or TAT control peptide (15 pmol/g, i.v.). Western blots were performed at 1 or 4 days post-injection. #p < 0.05, *p < 0.01, ANOVA.

See also Figures S5 and S6 and Movies S4, S5, S6, and S7.

receiving the PFC injection of p-cofilin peptide, but not TAT control peptide, displayed a significant increase in the preference of exploring the social stimulus over non-social object in phase 2 of sociability tests (p-cofilin peptide, social: 144.0 ± 5.2 s, nonsocial: 25.6 ± 1.5 s, n = 7; control peptide, social: 78.8 ± 12.6 s, nonsocial: 62.0 ± 13.8 s, n = 5, $F_{1,20\ (interaction)} = 36.7$, $p < 0.0001$, two-way ANOVA). The significantly increased social preference index in Shank3$^{+/\Delta C}$ mice after cofilin inhibition in PFC (Figure 5D, TAT control peptide: 15.2% ± 4.6%, n = 5, p-cofilin peptide: 69.9% ± 0.9%, n = 7, $p < 0.001$, t test) suggested the restored social interactions.

The systemic administration of cofilin inhibitory peptide led to the recovery of social behavior in Shank3$^{+/\Delta C}$ mice, which was consistent in each of the animals tested (Figure S5B). To determine whether the peptide may induce any side effects, we examined more behavioral tasks. As shown in Figure S5C, wild-type or Shank3$^{+/\Delta C}$ mice injected (i.v.) with TAT-p-cofilin peptide (15 pmol/g) exhibited normal performance in locomotion, open-field, and rotarod tests (n = 8–10 each group). The social preference was also unchanged in wild-type mice injected with TAT-p-cofilin peptide (WT: 62.7% ± 4.2%, n = 4, WT+p-cof pep: 59.9% ± 2.6%, n = 5). From the Movies S4, S6, and S7, it is also evident that Shank3$^{+/\Delta C}$ mice injected with the cofilin inhibitory peptide did not exhibit any behavioral abnormality or health problems, indicating that this reagent did not lead to the collapse of actin network in all cell types and induce unwanted side effects.

Furthermore, we examined the dose response of p-cofilin peptide. Administration (i.v.) of a low-dose p-cofilin peptide, which is 100-fold lower than the effective dose, 0.15 pmol/g, to Shank3$^{+/\Delta C}$ mice was incapable of ameliorating the social deficits (Figure S5D, phase 2, WT: 56.9% ± 1.9%, n = 4; Shank3$^{+/\Delta C}$: 11.9% ± 8.3%, n = 5, $p < 0.01$, t test) or repetitive grooming behaviors (Figure S5D, WT: 25.8 ± 10.4 s, n = 4; Shank3$^{+/\Delta C}$: 104.0 ± 24.1 s, n = 5, $p < 0.05$, t test).

Next, we tested whether inhibiting the activity of cofilin to block actin depolymerization could restore NMDAR function in *Shank3*-deficient mice. The NMDAR- to AMPAR-EPSC ratio in PFC neurons of Shank3$^{+/\Delta C}$ mice was significantly increased following (1 day) an i.v. injection of cofilin inhibitory peptide (Figure 5E, TAT control: 0.48 ± 0.03, n = 9, p-cofilin peptide: 0.68 ± 0.02, n = 10, $F_{3,30} = 23.2$, $p < 0.01$, one-way ANOVA), which was at the level similar to PFC neurons of wild-type mice injected with TAT control peptide (0.73 ± 0.03, n = 7). The p-cofilin peptide-induced recovery even persisted at 5 days post-injection (0.66 ± 0.02, n = 8, $p < 0.05$). Similarly, the input/output curves of NMDAR-EPSC also showed strong and sustained recovery in PFC neurons of Shank3$^{+/\Delta C}$ mice with an i.v. injection of TAT-p-cofilin peptide (Figure 5F, n = 20–24 each group, $F_{3,415\ (treatment)} = 26.6$, $p < 0.001$, two-way ANOVA). Furthermore, Shank3$^{+/\Delta C}$ mice with the stereotaxic injection of cofilin inhibitory peptide into PFC exhibited the significantly elevated NMDAR- to AMPAR-EPSC ratio (TAT control: 0.47 ± 0.04, n = 7, p-cofilin: 0.66 ± 0.04, n = 10, $p < 0.05$, t test) and NMDAR-EPSC input/output curves (Figure 5G, 50%–70% increase, n = 11–12 each group, $F_{1,105\ (treatment)} = 33.8$, $p < 0.001$, two-way ANOVA).

Biochemical experiments were also performed to examine the effect of cofilin inhibitor on synaptic NMDAR subunits in *Shank3*-deficient mice. As shown in Figures 5H and 5I, an injection (i.v.) of TAT-p-cofilin peptide (15 pmol/g) significantly elevated the levels of NR1 and NR2A in the synaptic membrane fraction of frontal cortical tissues of Shank3$^{+/\Delta C}$ mice, and this rescuing effect could still be observed at 4 days after injection (n = 4–7 per group, $p > 0.05$, ANOVA, compared to WT). Taken together, these results suggest that inhibiting cofilin to stabilize F-actin in PFC is able to provide a sustained rescue of the ASD-like behavioral deficits and NMDAR hypofunction in *Shank3*-deficient mice.

Additional electrophysiological experiments found that wild-type mice injected (i.v.) with TAT-p-cofilin peptide had largely unchanged NMDAR-EPSC in PFC neurons (Figure S6A, n = 16 pairs, $F_{1,155} = 1.7$, $p > 0.05$, two-way ANOVA) or striatal neurons (Figure S6B, n = 12 pairs, $F_{1,120} = 1.9$, $p > 0.05$, two-way ANOVA). Repetitive (once daily, 4 days) injections (i.v.) of TAT-p-cofilin peptide also led to the robust recovery of NMDAR-EPSC in PFC neurons of Shank3$^{+/\Delta C}$ mice (Figure S6C, n = 17–18 each group, $F_{1,160\ (treatment)} = 25.3$, $p < 0.001$, two-way ANOVA). Restoration of NMDAR-EPSC in hippocampal CA1 neurons of Shank3$^{+/\Delta C}$ mice was also observed with an i.v. injection of TAT-p-cofilin peptide (Figure S6D, n = 7–9 each group, $F_{2,100} = 2.2$, $p > 0.05$, two-way ANOVA). Moreover, NMDAR-EPSC was not restored by the low-dose p-cofilin peptide (Figure S6E, $F_{1,80} = 22.8$, n = 8–10 each group, $p < 0.001$, two-way ANOVA), probably due to its inability to inhibit cofilin activity.

PAK and Rac1 Are Involved in ASD-like Behavioral and Physiological Changes

One of the main upstream kinases for cofilin is PAK. PAK, by phosphorylating cofilin via LIMK, inhibits the ability of cofilin to depolymerize F-actin (Sells et al., 1997; Arber et al., 1998). Thus, we examined the role of PAK in ASD-like social behaviors. To inhibit PAK activity, we used PAK18, a 18-mer peptide against the proline-rich domain of PAK that blocks the PAK-PIX interaction essential for the PAK activation (Maruta et al., 2002). TAT-PAK18 (15 pmol/g) was i.v. injected into wide-type mice, followed by the test of social preference. Biochemical assays demonstrated that TAT-PAK18 peptide injection induced a significant reduction of endogenous PAK activity (p-PAK) and the downstream p-cofilin (inactive) level in PFC (Figures 6A and 6B). After TAT-PAK18 peptide injection, wild-type mice displayed a significant decrease in the preference of exploring the social stimulus over non-social object in phase 2 of sociability tests (Figure 6C, PAK18 peptide, social: 82.5 ± 7.0 s, nonsocial: 41.6 ± 3.3 s, n = 11; TAT control peptide, social: 172.3 ± 7.7 s, nonsocial: 38.7 ± 5.9 s, n = 9, $F_{1,36\ (interaction)} = 57.6$, $p < 0.0001$, two-way ANOVA). The significantly decreased social preference index (phase 2) in WT mice after PAK inhibition (Figure 6D, TAT: 64.0% ± 4.5%, n = 9; PAK18: 31.5% ± 4.7%, n = 11, $p < 0.01$, t test) suggested the decreased social affiliation.

In parallel with the induction of ASD-like behavioral deficits with PAK inhibition, the synaptic NMDAR function was also significantly diminished in PFC neurons from wild-type mice injected with PAK18 peptide (Figure 6E, 20%–30% decrease, n = 11–12 each group, $F_{1,105\ (treatment)} = 31.7$, $p < 0.001$, two-way ANOVA). These data suggest that PAK inhibition could lead to behavioral and physiological impairment reminiscent of autism.

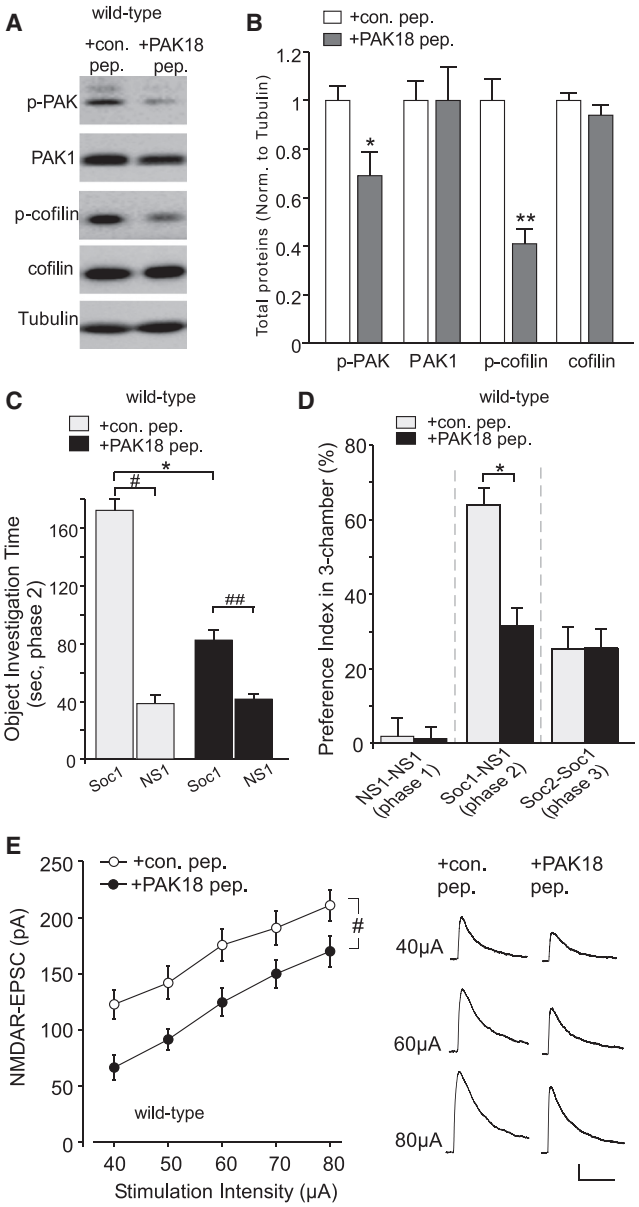

Figure 6. Inhibition of PAK Induces Social Deficits and NMDAR Hypofunction in Wild-Type Mice

(A and B) Immunoblots and quantification (mean ± SEM) of p-PAK, PAK1, p-cofilin, and cofilin in PFC slices from WT mice injected with TAT-PAK18 inhibitory peptide (15 pmol/g, i.v.) or TAT control peptide. *p < 0.05, **p < 0.01, t test.

(C and D) Bar graphs (mean ± SEM) showing the time spent investigating either the social or nonsocial stimulus during phase 2 of sociability testing (C) and the preference index at three phases of sociability testing (D) in WT mice injected with TAT-PAK18 or TAT control peptide. *p < 0.001, control versus PAK18 peptide; #p < 0.001, ##p < 0.01, Soc1 versus NS1, two-way ANOVA (C). *p < 0.01, t test (D).

(E) Input-output curves (mean ± SEM) of NMDAR-EPSC in WT mice injected with TAT-PAK18 or TAT control peptide. #p < 0.05, ANOVA. Inset: representative NMDAR-EPSC traces.

Scale bars, 40 pA, 200 ms.

One of the major upstream regulators of PAK involved in actin cytoskeletal rearrangements is Rac1. To examine the role of Rac1 in autism, we manipulated the activity of Rac1 using herpes simplex virus (HSV)-mediated gene transfer (Dietz et al., 2012). HSV constructs containing fluorescent protein-tagged dominant-negative Rac1 (DN-Rac1) or constitutively active Rac1 (CA-Rac1) were bilaterally injected into prelimbic regions (Figure 7A). Viral expression of DN-Rac1 in wild-type mice induced ASD-like social deficits in the three-chamber social interaction assay, which was reflected by a significantly lower preference index for the social stimulus over the non-social object in phase 2 (Figure 7B, GFP control in WT: 57.4% ± 4.6%, n = 7; DN-Rac1 in WT: 16.2% ± 6.7%, n = 6, $p < 0.001$, t test). Conversely, viral expression of CA-Rac1 in Shank3$^{+/\Delta C}$ mice rescued the ASD-like social deficits in the three-chamber social interaction assay, which was reflected by a significantly higher preference index for the social stimulus over the non-social object in phase 2 (Figure 7C, GFP control in Shank3$^{+/\Delta C}$: 16.1% ± 3.7%, n = 4; CA-Rac1 in Shank3$^{+/\Delta C}$: 67.5% ± 2.0%, n = 4, $p < 0.001$, t test).

Electrophysiological experiments were also performed on mice with in vivo manipulation of Rac1 activity in PFC. As shown in Figure 7D, NMDAR-EPSC was markedly reduced in PFC pyramidal neurons from WT mice injected with DN-Rac1 HSV (30%–40% decrease, n = 12–14 each group, $F_{1,120\ (treatment)} = 50.2$, $p < 0.001$, two-way ANOVA). Furthermore, NMDAR-EPSC was significantly increased in PFC pyramidal neurons from Shank3$^{+/\Delta C}$ mice injected with CA-Rac1 HSV (Figure 7E, 40%–60% increase, n = 14–15 each group, $F_{1,135\ (treatment)} = 28.9$, $p < 0.001$, two-way ANOVA). Taken together, these results suggest that the ASD-like behavioral and physiological deficits can be induced by Rac1 inhibition in normal animals, and can be rescued by Rac1 activation in *Shank3*-deficient conditions.

DISCUSSION

Transcriptomic analyses of ASD brains have revealed that gene mutations that lead to synaptic and neuronal signaling dysfunction are a convergent molecular pathology of autism (Voineagu et al., 2011; Gilman et al., 2011). The gene expression changes associated with ASD are most pronounced in the frontal cortex (Voineagu et al., 2011). The impairments of PFC-mediated executive functions in individuals with ASD, including cognitive flexibility, social interaction, inhibition, planning, and attention (Anderson et al., 1999; Hill, 2004), suggest that genetic changes that cause synaptic dysfunction in frontal cortex may be at the heart of autism.

The *Shank3* gene, located on chromosome 22q13.3 in humans, was first implicated in ASD from genetic analysis of the 22q13.3 microdeletion syndrome. Heterozygous mutations in *Shank3* gene cause ASD in a gene-dosage dependent manner (Durand et al., 2007; Sebat et al., 2007). Heterozygous mice expressing C-terminal deleted Shank3, Shank3$^{+/\Delta C}$, had a marked deficiency of the endogenous full-length Shank3 isoforms (Figure 1A), providing a model of autism with the loss of naturally occurring Shank3 proteins. Interestingly, we found that juvenile male *Shank3*-deficient mice exhibited ASD-like behavioral deficits, including social interaction deficiency (Figures 1B and 1C) and repetitive grooming (Figure 1D). Some of the phenotypes

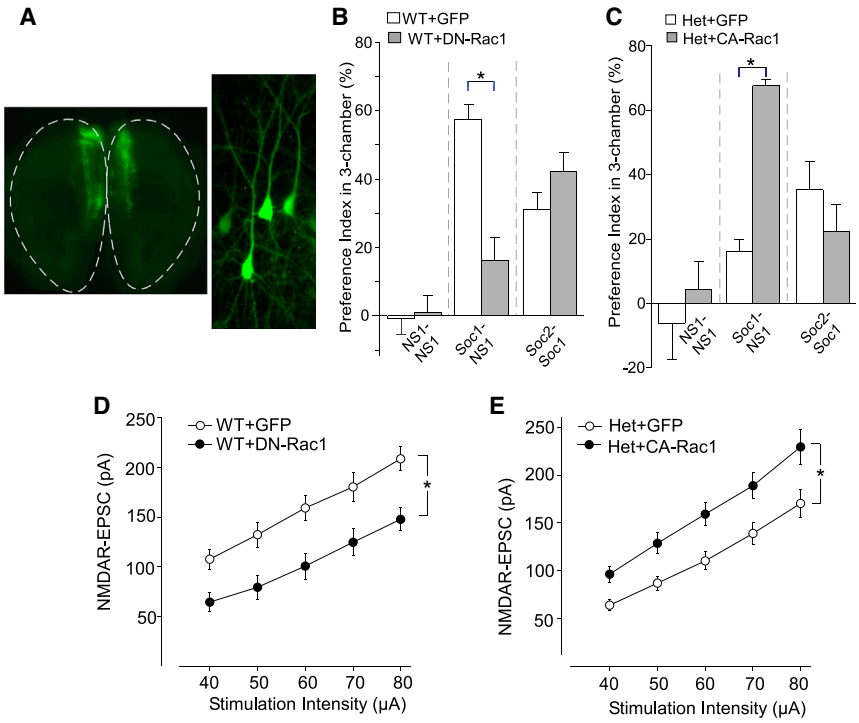

Figure 7. Social Deficits and NMDAR Hypofunction Are Induced by Suppressing Rac1 Activity in Wild-Type Mice and Rescued by Elevating Rac1 Activity in *Shank3*-Deficient Mice

(A) A low-magnification (5×) image of a coronal slice showing the GFP HSV-infected medial PFC region. Inset: a confocal image (40×) of HSV-infected PFC neurons.

(B and C) Bar graphs (mean ± SEM) showing the preference index for three phases of sociability testing in WT mice with PFC injection of dominant-negative Rac1 (DN-Rac1) HSV (B), or in Shank3$^{+/\Delta C}$ mice with PFC injection of constitutively active Rac1 (CA-Rac1) HSV (C). GFP HSV was used as a control. *p < 0.01, t test.

(D and E) Input-output curves (mean ± SEM) of NMDAR-EPSC in WT mice with PFC injection of DN-Rac1 HSV (D) or in Shank3$^{+/\Delta C}$ mice with PFC injection of CA-Rac1 HSV (E). *p < 0.01, ANOVA.

have also been observed in animals carrying other Shank3 deletions/mutations (Jiang and Ehlers, 2013). However, the phenotypes of Shank3 mutant mice are not always consistent, with either significant (Wang et al., 2011; Peça et al., 2011) or mild (Bozdagi et al., 2010; Kouser et al., 2013) social deficits being reported. Potential contributing factors for the discrepancy include the different locations of the *Shank3* gene mutation and the different methods utilized in habituating and testing animals.

Blocking NMDA receptors in the PFC of wild-type mice induced ASD-like social deficits (Figures 1E and 1F), suggesting that the behavioral abnormality in Shank3$^{+/\Delta C}$ mice might be caused by NMDAR hypofunction. In agreement with this, we have found a selective loss of NMDAR-mediated synaptic response in PFC neurons of Shank3$^{+/\Delta C}$ mice (Figures 2A–2C). Consistently, homozygous Shank3$^{\Delta C/\Delta C}$ mice exhibit reduced NMDAR to AMPAR-EPSC ratio and impairments in hippocampal synaptic transmission and plasticity (Kouser et al., 2013). Drugs acting at the glycine site on the NMDAR to enhance its function have been found to have therapeutic potential for autism treatment (Won et al., 2012). The NMDAR hypofunction in Shank3$^{+/\Delta C}$ mice was associated with the reduced level of synaptic NMDAR subunits (Figures 2D and 2E), suggesting the impairment of NMDAR synaptic trafficking by Shank3 deficiency.

Previous studies have shown that NMDAR membrane delivery and stability is dependent on the integrity of actin cytoskeleton (Rosenmund and Westbrook, 1993; Allison et al., 1998; Morishita et al., 2005; Duffney et al., 2013). Abnormalities in Rho GTPase signaling, which orchestrate coordinated changes in actin assembly and organization (Hall, 1998; Calabrese et al., 2006), have been identified as a prominent cause of mental retardation (Allen et al., 1998; Ramakers, 2002). Shank forms a complex with βPIX, the GEF involved in Rac1 activation, and overexpression of Shank in cultured neurons promotes synaptic accumulation of βPIX (Park et al., 2003). We found that, in cortical slices of Shank3$^{+/\Delta C}$ mice (Figure 3), the expression of βPIX was strongly reduced, which led to the decreased Rac1 activity. The Rac1 downstream effectors, active (phosphorylated) PAK and LIMK, were significantly reduced in Shank3$^{+/\Delta C}$ mice. Moreover, cofilin, the major actin depolymerizing factor that is phosphorylated and inactivated by PAK/LIMK signaling, was disinhibited. Consequently, the level of F-actin was substantially decreased in PFC of *Shank3*-deficient mice, which was likely due to the increased cofilin activity (Figure 4). Examination of actin signaling in another *Shank3*-deficient mouse line that lacks the longest isoforms of Shank3 also demonstrated multiple changes in actin signaling including decreased LIMK and phosphorylated (inactive) cofilin (Figure S4B).

In corroboration with our results, overexpression of Shank3 has been found to enhance actin polymerization (Durand et al., 2012) and increase F-actin levels (Han et al., 2013). The alterations of actin regulators in Shank3 models of autism identified in this study also supports the genetic analysis of autistic brains, which suggests that autism-associated de novo variants converge on the genes involved in the regulation of actin filaments and the formation and function of synapses (Gilman et al., 2011).

To determine whether the dysregulation of synaptic actin cytoskeleton drives autistic phenotypes in *Shank3*-deficient mice, we perturbed key actin regulators. Inhibition of cofilin activity produced a robust and long-lasting rescue of the social interaction deficits and repetitive behavior in Shank3$^{+/\Delta C}$ mice (Figure 5), which correlated well with the restoration of NMDAR function, suggesting a promising therapeutic strategy for autism treatment. No behavioral abnormality or health problems have been observed in Shank3$^{+/\Delta C}$ mice injected with the cofilin inhibitory

peptide, suggesting that it is a safe and effective intervention. Although local injections of the cofilin inhibitor to prefrontal cortex of Shank3$^{+/\Delta C}$ mice led to similar rescue of autistic behaviors, systemic (i.v.) injections provide a much more feasible therapeutic approach.

Inhibiting PAK or Rac1 function in wild-type animals produced ASD-like social deficits and NMDAR hypofunction (Figures 6, 7B, and 7D), confirming the importance of Rac1/PAK signaling in autism. Indeed, elevating Rac1 activity in PFC of *Shank3*-deficient mice also led to the rescue of behavioral and NMDAR abnormality (Figures 7C and 7E), providing another molecular target for autism treatment.

Given the universal expression of actin in all cell types, one concern is the potential non-specific effects generated by actin manipulating agents. However, some actin regulators are largely brain specific, such as the ASD risk gene *CTTNBP2* (De Rubeis et al., 2014), which interacts with the F-actin-binding protein Cortactin (a Shank3 binding protein). Actin filament is highly enriched and forms a uniquely dynamic structure in dendritic spines of neurons (Frost et al., 2010), serving a special role to regulate the formation, maintenance, and function of glutamatergic synapses during development and at mature stages (Matus, 2000; Hotulainen and Hoogenraad, 2010). Different postsynaptic proteins are differentially affected by actin dynamics, with NMDARs being very sensitive to the state of actin depolymerization. Moreover, Shank3 directly links NMDARs to actin cytoskeleton, making NMDARs particularly sensitive to Shank3-induced changes in actin dynamics. It is probably the reason why AMPARs, which can also be regulated by actin (Rocca et al., 2008; Yuen et al., 2010), are not significantly affected in *Shank3*-deficient neurons. High-throughput gene expression profiling has found that different actin interacting proteins have distinct transcriptional activity in different brain regions and non-CNS areas, thus targeting the actin regulators highly restricted to PFC, such as human PAK3, whose mutation causes X-linked mental retardation (Allen et al., 1998), will enable the specific normalization of actin dynamics at PFC glutamatergic synapses.

In summary, our convergent evidence has revealed actin dysregulation and ensuing NMDAR hypofunction in pyramidal neurons of prefrontal cortex as a pathophysiological basis for the ASD-like behaviors in a Shank3 model of autism. Normally, Shank3 crosslinks NMDARs to the actin cytoskeleton. Loss of Shank3 leads to the reduced expression of βPIX (GEF for Rac1) and reduced Rac1/PAK/LIMK signaling, which results in the increased cofilin activity (due to reduced cofilin phosphorylation). Consequently, actin depolymerization is increased, leading to disrupted NMDAR synaptic delivery through the actin cytoskeleton. The loss of functional NMDARs in PFC contributes to autism-like social deficits. In support of our findings, anatomical studies have found focal patches of abnormal organization in prefrontal cortex of autistic children, with the clearest deficits in the expression of markers of excitatory cortical neurons in layers 4 and 5 (Stoner et al., 2014). Genetic analyses have found enriched mutations in genes regulating actin filament network at glutamatergic synapses in autism (Gilman et al., 2011). Our results also suggest that perturbing the signaling molecules in Rac1/PAK/cofilin pathway to normalize cortical actin dynamics offers a potential therapeutic strategy to ameliorate behavioral and synaptic defects in autism.

EXPERIMENTAL PROCEDURES

All experiments were performed with the approval of the Institutional Animal Care and Use Committee of the State University of New York at Buffalo.

Behavioral Testing and Animal Surgery

The mice expressing C-terminal (exon 21) deleted Shank3 (Jackson Laboratory) were generated as previously described (Kouser et al., 2013). Heterozygous Shank3$^{+/\Delta C}$ mice (6–8 weeks old, male) and age-matched wild-type mice (C57BL/6, male) were mainly used in this study. For details on behavioral assays, including social preference, locomotion, open-field, rotarod, and self-grooming, and animal surgery details, see the Supplemental Experimental Procedures.

Electrophysiological Recordings

Whole-cell voltage-clamp recording technique was used to measure synaptic currents in layer 5 pyramidal neurons of prefrontal cortical slices, as previously described (Yuen et al., 2012). See the Supplemental Experimental Procedures for details.

Biochemical Measurements, Immunohistochemistry, and 2D-DIGE

See the Supplemental Experimental Procedures for details.

Statistics

All data are expressed as the mean ± SEM. Experiments with two groups were analyzed statistically using unpaired Student's t tests. Experiments with more than two groups were subjected to one-way ANOVA, two-way ANOVA, or two-way repeated-measure ANOVA (rmANOVA), followed by post hoc Bonferroni tests.

SUPPLEMENTAL INFORMATION

Supplemental Information includes Supplemental Experimental Procedures, Supplemental Results, Supplemental Discussion, seven figures, and seven movies and can be found with this article online at http://dx.doi.org/10.1016/j.celrep.2015.04.064.

AUTHOR CONTRIBUTIONS

L.J.D. performed behavioral tests and immunocytochemical and imaging experiments, analyzed the data, and wrote parts of the paper. P.Z. and J.C. performed electrophysiological analyses. J.W. and E.M. performed biochemical assays. L.Q. performed Golgi staining. K.M. performed some behavioral tests. D.M.D. contributed to the design of biochemical experiments. Y.K. and J.D.B. performed biochemical assays in a different Shank3 mouse model. Z.Y. designed experiments, supervised the project, and wrote the paper.

ACKNOWLEDGMENTS

We thank Xiaoqing Chen for excellent technical support. We are grateful to Dr. Eric Nestler (Icahn School of Medicine at Mount Sinai) for providing mutant Rac1 herpes simplex viruses and Dr. Tobias Boeckers (Ulm University, Germany) for providing Shank3 C-term antibody. This work was supported by NIH grant MH101690 to Z.Y. and the Seaver Foundation and NIH grant MH093725 to J.D.B.

Received: June 25, 2014
Revised: March 5, 2015
Accepted: April 30, 2015
Published: May 28, 2015

REFERENCES

Aarts, M., Liu, Y., Liu, L., Besshoh, S., Arundine, M., Gurd, J.W., Wang, Y.T., Salter, M.W., and Tymianski, M. (2002). Treatment of ischemic brain damage by perturbing NMDA receptor- PSD-95 protein interactions. Science *298*, 846–850.

Allen, K.M., Gleeson, J.G., Bagrodia, S., Partington, M.W., MacMillan, J.C., Cerione, R.A., Mulley, J.C., and Walsh, C.A. (1998). PAK3 mutation in nonsyndromic X-linked mental retardation. Nat. Genet. *20*, 25–30.

Allison, D.W., Gelfand, V.I., Spector, I., and Craig, A.M. (1998). Role of actin in anchoring postsynaptic receptors in cultured hippocampal neurons: differential attachment of NMDA versus AMPA receptors. J. Neurosci. *18*, 2423–2436.

Anderson, S.W., Bechara, A., Damasio, H., Tranel, D., and Damasio, A.R. (1999). Impairment of social and moral behavior related to early damage in human prefrontal cortex. Nat. Neurosci. *2*, 1032–1037.

Arber, S., Barbayannis, F.A., Hanser, H., Schneider, C., Stanyon, C.A., Bernard, O., and Caroni, P. (1998). Regulation of actin dynamics through phosphorylation of cofilin by LIM-kinase. Nature *393*, 805–809.

Bamburg, J.R. (1999). Proteins of the ADF/cofilin family: essential regulators of actin dynamics. Annu. Rev. Cell Dev. Biol. *15*, 185–230.

Betancur, C., and Buxbaum, J.D. (2013). SHANK3 haploinsufficiency: a "common" but underdiagnosed highly penetrant monogenic cause of autism spectrum disorders. Mol Autism *4*, 17.

Bonaglia, M.C., Giorda, R., Borgatti, R., Felisari, G., Gagliardi, C., Selicorni, A., and Zuffardi, O. (2001). Disruption of the ProSAP2 gene in a t(12;22)(q24.1;q13.3) is associated with the 22q13.3 deletion syndrome. Am. J. Hum. Genet. *69*, 261–268.

Borsello, T., Clarke, P.G., Hirt, L., Vercelli, A., Repici, M., Schorderet, D.F., Bogousslavsky, J., and Bonny, C. (2003). A peptide inhibitor of c-Jun N-terminal kinase protects against excitotoxicity and cerebral ischemia. Nat. Med. *9*, 1180–1186.

Bozdagi, O., Sakurai, T., Papapetrou, D., Wang, X., Dickstein, D.L., Takahashi, N., Kajiwara, Y., Yang, M., Katz, A.M., Scattoni, M.L., et al. (2010). Haploinsufficiency of the autism-associated Shank3 gene leads to deficits in synaptic function, social interaction, and social communication. Mol Autism *1*, 15.

Calabrese, B., Wilson, M.S., and Halpain, S. (2006). Development and regulation of dendritic spine synapses. Physiology (Bethesda) *21*, 38–47.

Carlson, G.C. (2012). Glutamate receptor dysfunction and drug targets across models of autism spectrum disorders. Pharmacol. Biochem. Behav. *100*, 850–854.

De Rubeis, S., He, X., Goldberg, A.P., Poultney, C.S., Samocha, K., Cicek, A.E., Kou, Y., Liu, L., Fromer, M., Walker, S., et al.; DDD Study; Homozygosity Mapping Collaborative for Autism; UK10K Consortium (2014). Synaptic, transcriptional and chromatin genes disrupted in autism. Nature *515*, 209–215.

Dietz, D.M., Sun, H., Lobo, M.K., Cahill, M.E., Chadwick, B., Gao, V., Koo, J.W., Mazei-Robison, M.S., Dias, C., Maze, I., et al. (2012). Rac1 is essential in cocaine-induced structural plasticity of nucleus accumbens neurons. Nat. Neurosci. *15*, 891–896.

dos Remedios, C.G., Chhabra, D., Kekic, M., Dedova, I.V., Tsubakihara, M., Berry, D.A., and Nosworthy, N.J. (2003). Actin binding proteins: regulation of cytoskeletal microfilaments. Physiol. Rev. *83*, 433–473.

Duffney, L.J., Wei, J., Cheng, J., Liu, W., Smith, K.R., Kittler, J.T., and Yan, Z. (2013). Shank3 deficiency induces NMDA receptor hypofunction via an actin-dependent mechanism. J. Neurosci. *33*, 15767–15778.

Durand, C.M., Betancur, C., Boeckers, T.M., Bockmann, J., Chaste, P., Fauchereau, F., Nygren, G., Rastam, M., Gillberg, I.C., Anckarsäter, H., et al. (2007). Mutations in the gene encoding the synaptic scaffolding protein SHANK3 are associated with autism spectrum disorders. Nat. Genet. *39*, 25–27.

Durand, C.M., Perroy, J., Loll, F., Perrais, D., Fagni, L., Bourgeron, T., Montcouquiol, M., and Sans, N. (2012). SHANK3 mutations identified in autism lead to modification of dendritic spine morphology via an actin-dependent mechanism. Mol. Psychiatry *17*, 71–84.

Ehlers, M.D. (1999). Synapse structure: glutamate receptors connected by the shanks. Curr. Biol. *9*, R848–R850.

Fromer, M., Pocklington, A.J., Kavanagh, D.H., Williams, H.J., Dwyer, S., Gormley, P., Georgieva, L., Rees, E., Palta, P., Ruderfer, D.M., et al. (2014). De novo mutations in schizophrenia implicate synaptic networks. Nature *506*, 179–184.

Frost, N.A., Shroff, H., Kong, H., Betzig, E., and Blanpied, T.A. (2010). Single-molecule discrimination of discrete perisynaptic and distributed sites of actin filament assembly within dendritic spines. Neuron *67*, 86–99.

Fukazawa, Y., Saitoh, Y., Ozawa, F., Ohta, Y., Mizuno, K., and Inokuchi, K. (2003). Hippocampal LTP is accompanied by enhanced F-actin content within the dendritic spine that is essential for late LTP maintenance in vivo. Neuron *38*, 447–460.

Gilman, S.R., Iossifov, I., Levy, D., Ronemus, M., Wigler, M., and Vitkup, D. (2011). Rare de novo variants associated with autism implicate a large functional network of genes involved in formation and function of synapses. Neuron *70*, 898–907.

Golden, S.A., Christoffel, D.J., Heshmati, M., Hodes, G.E., Magida, J., Davis, K., Cahill, M.E., Dias, C., Ribeiro, E., Ables, J.L., et al. (2013). Epigenetic regulation of RAC1 induces synaptic remodeling in stress disorders and depression. Nat. Med. *19*, 337–344.

Hall, A. (1998). Rho GTPases and the actin cytoskeleton. Science *279*, 509–514.

Han, K., Holder, J.L., Jr., Schaaf, C.P., Lu, H., Chen, H., Kang, H., Tang, J., Wu, Z., Hao, S., Cheung, S.W., et al. (2013). SHANK3 overexpression causes manic-like behaviour with unique pharmacogenetic properties. Nature *503*, 72–77.

Hayashi, M.L., Choi, S.Y., Rao, B.S., Jung, H.Y., Lee, H.K., Zhang, D., Chattarji, S., Kirkwood, A., and Tonegawa, S. (2004). Altered cortical synaptic morphology and impaired memory consolidation in forebrain- specific dominant-negative PAK transgenic mice. Neuron *42*, 773–787.

Hayashi, M.K., Tang, C., Verpelli, C., Narayanan, R., Stearns, M.H., Xu, R.M., Li, H., Sala, C., and Hayashi, Y. (2009). The postsynaptic density proteins Homer and Shank form a polymeric network structure. Cell *137*, 159–171.

Hill, E.L. (2004). Executive dysfunction in autism. Trends Cogn. Sci. *8*, 26–32.

Hotulainen, P., and Hoogenraad, C.C. (2010). Actin in dendritic spines: connecting dynamics to function. J. Cell Biol. *189*, 619–629.

Jiang, Y.H., and Ehlers, M.D. (2013). Modeling autism by SHANK gene mutations in mice. Neuron *78*, 8–27.

Kouser, M., Speed, H.E., Dewey, C.M., Reimers, J.M., Widman, A.J., Gupta, N., Liu, S., Jaramillo, T.C., Bangash, M., Xiao, B., et al. (2013). Loss of predominant Shank3 isoforms results in hippocampus-dependent impairments in behavior and synaptic transmission. J. Neurosci. *33*, 18448–18468.

Manser, E., Loo, T.H., Koh, C.G., Zhao, Z.S., Chen, X.Q., Tan, L., Tan, I., Leung, T., and Lim, L. (1998). PAK kinases are directly coupled to the PIX family of nucleotide exchange factors. Mol. Cell *1*, 183–192.

Maruta, H., He, H., and Nheu, T. (2002). Interfering with Ras signaling using membrane-permeable peptides or drugs. Methods Mol. Biol. *189*, 75–85.

Matus, A. (2000). Actin-based plasticity in dendritic spines. Science *290*, 754–758.

Morishita, W., Marie, H., and Malenka, R.C. (2005). Distinct triggering and expression mechanisms underlie LTD of AMPA and NMDA synaptic responses. Nat. Neurosci. *8*, 1043–1050.

Naisbitt, S., Kim, E., Tu, J.C., Xiao, B., Sala, C., Valtschanoff, J., Weinberg, R.J., Worley, P.F., and Sheng, M. (1999). Shank, a novel family of postsynaptic density proteins that binds to the NMDA receptor/PSD-95/GKAP complex and cortactin. Neuron *23*, 569–582.

Park, E., Na, M., Choi, J., Kim, S., Lee, J.R., Yoon, J., Park, D., Sheng, M., and Kim, E. (2003). The Shank family of postsynaptic density proteins interacts with and promotes synaptic accumulation of the beta PIX guanine nucleotide exchange factor for Rac1 and Cdc42. J. Biol. Chem. *278*, 19220–19229.

Peça, J., Feliciano, C., Ting, J.T., Wang, W., Wells, M.F., Venkatraman, T.N., Lascola, C.D., Fu, Z., and Feng, G. (2011). Shank3 mutant mice display autistic-like behaviours and striatal dysfunction. Nature *472*, 437–442.

Ramakers, G.J. (2002). Rho proteins, mental retardation and the cellular basis of cognition. Trends Neurosci. *25*, 191–199.

Ridley, A.J. (2006). Rho GTPases and actin dynamics in membrane protrusions and vesicle trafficking. Trends Cell Biol. *16*, 522–529.

Rocca, D.L., Martin, S., Jenkins, E.L., and Hanley, J.G. (2008). Inhibition of Arp2/3-mediated actin polymerization by PICK1 regulates neuronal morphology and AMPA receptor endocytosis. Nat. Cell Biol. *10*, 259–271.

Rosenmund, C., and Westbrook, G.L. (1993). Calcium-induced actin depolymerization reduces NMDA channel activity. Neuron *10*, 805–814.

Sala, C., Piëch, V., Wilson, N.R., Passafaro, M., Liu, G., and Sheng, M. (2001). Regulation of dendritic spine morphology and synaptic function by Shank and Homer. Neuron *31*, 115–130.

Sebat, J., Lakshmi, B., Malhotra, D., Troge, J., Lese-Martin, C., Walsh, T., Yamrom, B., Yoon, S., Krasnitz, A., Kendall, J., et al. (2007). Strong association of de novo copy number mutations with autism. Science *316*, 445–449.

Sells, M.A., Knaus, U.G., Bagrodia, S., Ambrose, D.M., Bokoch, G.M., and Chernoff, J. (1997). Human p21-activated kinase (Pak1) regulates actin organization in mammalian cells. Curr. Biol. *7*, 202–210.

Sheng, M., and Kim, E. (2000). The Shank family of scaffold proteins. J. Cell Sci. *113*, 1851–1856.

Stoner, R., Chow, M.L., Boyle, M.P., Sunkin, S.M., Mouton, P.R., Roy, S., Wynshaw-Boris, A., Colamarino, S.A., Lein, E.S., and Courchesne, E. (2014). Patches of disorganization in the neocortex of children with autism. N. Engl. J. Med. *370*, 1209–1219.

ten Klooster, J.P., Jaffer, Z.M., Chernoff, J., and Hordijk, P.L. (2006). Targeting and activation of Rac1 are mediated by the exchange factor beta-Pix. J. Cell Biol. *172*, 759–769.

Threadgill, R., Bobb, K., and Ghosh, A. (1997). Regulation of dendritic growth and remodeling by Rho, Rac, and Cdc42. Neuron *19*, 625–634.

Voineagu, I., Wang, X., Johnston, P., Lowe, J.K., Tian, Y., Horvath, S., Mill, J., Cantor, R.M., Blencowe, B.J., and Geschwind, D.H. (2011). Transcriptomic analysis of autistic brain reveals convergent molecular pathology. Nature *474*, 380–384.

Wang, X., McCoy, P.A., Rodriguiz, R.M., Pan, Y., Je, H.S., Roberts, A.C., Kim, C.J., Berrios, J., Colvin, J.S., Bousquet-Moore, D., et al. (2011). Synaptic dysfunction and abnormal behaviors in mice lacking major isoforms of Shank3. Hum. Mol. Genet. *20*, 3093–3108.

Won, H., Lee, H.R., Gee, H.Y., Mah, W., Kim, J.I., Lee, J., Ha, S., Chung, C., Jung, E.S., Cho, Y.S., et al. (2012). Autistic-like social behaviour in Shank2-mutant mice improved by restoring NMDA receptor function. Nature *486*, 261–265.

Wyszynski, M., Lin, J., Rao, A., Nigh, E., Beggs, A.H., Craig, A.M., and Sheng, M. (1997). Competitive binding of α-actinin and calmodulin to the NMDA receptor. Nature *385*, 439–442.

Yuen, E.Y., Liu, W., Kafri, T., van Praag, H., and Yan, Z. (2010). Regulation of AMPA receptor channels and synaptic plasticity by cofilin phosphatase Slingshot in cortical neurons. J. Physiol. *588*, 2361–2371.

Yuen, E.Y., Wei, J., Liu, W., Zhong, P., Li, X., and Yan, Z. (2012). Repeated stress causes cognitive impairment by suppressing glutamate receptor expression and function in prefrontal cortex. Neuron *73*, 962–977.

Zou, H., Zhang, C., Xie, Q., Zhang, M., Shi, J., Jin, M., and Yu, L. (2008). Low dose MK-801 reduces social investigation in mice. Pharmacol. Biochem. Behav. *90*, 753–757.